Collective dynamics of coupled Lorenz oscillators near the Hopf boundary: Intermittency and chimera states

Anjuman Ara Khatun [1,2] Yusra Ahmed Muthanna [1,3] Nirmal Punetha [4] and Haider Hasan Jafri[1]

[1]*Department of Physics, Aligarh Muslim University, Aligarh 202 002, India*
[2]*Department of Physics, Indian Institute of Technology Bombay, Mumbai 400 076, India*
[3]*Physics Department, Taiz University, Taiz 6803, Yemen*
[4]*Amity University Haryana, Gurgaon 122413, India*

We study collective dynamics of networks of mutually coupled identical Lorenz oscillators near a subcritical Hopf bifurcation. Such systems exhibit induced multistable behavior with interesting spatiotemporal dynamics including synchronization, desynchronization, and chimera states. For analysis, we first consider a ring topology with nearest-neighbor coupling and find that the system may exhibit intermittent behavior due to the complex basin structures and dynamical frustration, where temporal dynamics of the oscillators in the ensemble switches between different attractors. Consequently, different oscillators may show a dynamics that is intermittently synchronized (or desynchronized), giving rise to *intermittent chimera states*. The behavior of the intermittent laminar phases is characterized by the characteristic time spent in the synchronization manifold, which decays as a power law. Such intermittent dynamics is quite general and is also observed in an ensemble of a large number of oscillators arranged in variety of network topologies including nonlocal, scale-free, random, and small-world networks.

I. INTRODUCTION

For many decades now, the Lorenz equations [1],

$$\dot{x} = \rho(y - x), \quad \dot{y} = \gamma x - y - xz, \quad \dot{z} = xy - \beta z, \quad (1)$$

used for describing convection rolls in the atmosphere, have served as a paradigmatic model to study dynamical properties of chaotic systems. Typical parameter values considered in such studies [2], e.g., $\rho = 10$, $\gamma = 28$, and $\beta = 8/3$, ensure asymptotic motion on a well-known Lorenz chaotic attractor. This dynamically rich model has been used in a number of studies as a standard prototype for exploring properties of chaotic dynamics [2] and phenomena such as chaos synchronization [3–6], amplitude death [7,8], chimera dynamics [9–11], and intermittency [10,12].

The idea that chaotic systems can be driven to synchrony was introduced by Pecora and Carroll [3]. Since then different scenarios of synchronization have been extensively studied in a wide range of periodic and chaotic systems with various coupling strategies [13–16]. These include generalized synchrony [17], complete [3,18], and phase and lag synchrony [19]. The study of the phenomenon of synchronization, due to its ubiquitous presence in wide range of real-world systems, has found applications in various fields including physics, biology, social sciences, and engineering [20].

A related phenomenon which is observed close to the boundary of chaotic synchrony is intermittency. This interesting dynamics refers to a situation where phase-synchronized oscillations (laminar phases) are interrupted by nonsynchronous behavior (phase slips) during persistent time intervals. Intermittency is observed close to the threshold

parameter values for which the coupled system is synchronized. Various studies have explored its origin and statistical properties, and different types of intermittent behaviors have been classified as type I, II [21,22], or on-off intermittency [23,24]. These pretransitional intermittencies have been characterized near lag [19,25,26], generalized [27], and phase [28–31] synchronization regimes. Essentially, intermittency is an irregular alternation of phases of apparently periodic and chaotic dynamics (Pomeau-Manneville dynamics) or different forms of chaotic dynamics (crisis-induced intermittency). The classic type I, II, and III intermittencies (Pomeau and Manneville [32]) involve the motion alternating between laminar and chaotic states characterized by the scaling exponents of the duration spent in one (or the other) state when a parameter is varied. Other forms of intermittencies include crisis-induced [33], type V [34], on-off [23], in-out [35], etc. The statistics of distributions of Lyapunov exponents has been applied to the case of intermittency [36,37]. Studies have shown that switching of dynamics between two or more distinct types of behavior reflects the distribution of largest Lyapunov exponents (LLEs) [36].

An interesting spatiotemporal pattern called the chimera state is another collective behavior observed in ensembles of oscillators. In this state, the oscillator population spontaneously splits into synchronized and desynchronized populations, breaking its symmetry [38–40]. Recently, these states have gained great interest due to their interesting spatiotemporal nature with two dynamically distinct properties, namely, synchronized and desynchronized motions, coexisting in a single population. These mixed states have applications in understanding phenomena such as ventricular

fibrillation, unihemispheric and REM (rapid eye movement) sleep, power grid stability, and consensus formations in social networks [40].

Chimera states are observed in several oscillator ensembles from large oscillator networks where a thermodynamic limit can be applied [38,39] to a network as small as a system of three oscillators [41–49]. In general, chimera states in oscillator ensembles are known to emerge when some degree of nonuniformity is introduced in the system [40], for example, in the form of nonlocal interactions [38,39], modularity [50–53], parameter heterogeneities [54,55], time-delay couplings [56], or amplitude fluctuations [57]. However, recent studies suggest that even in the absence of such nonuniformities, in a globally coupled ensemble of identical chaotic oscillators, chimeric states can be generated [9,58] and controlled [59,60] through induced multistability. In this case interactions between the oscillators modify effective control parameters of the system, thus shifting it towards a multistable regime where attractors with contrasting synchronization properties coexist. In this multistable regime, depending on the initial conditions, the oscillators from the population can settle into any of these coexisting attractors with dynamically different properties. Since both synchronized and desynchronized motions are possible on these attractors, the system exhibits chimeric behavior. The basins of attraction in such systems were found to be interwoven and riddled [58] with a multiplicity of coexisting attractors [61].

The interplay between structural properties of a network and the dynamics of the individual units is crucial in understanding its resulting behavior. In this work, we investigate the robustness of multistability-induced chimera states for different network topologies, specifically, when there is a frustration effect in the network. These chimera states—observed for mean field interactions (global coupling)—are sensitive to, among other factors, the nature of the coupling and how far the system is from the Hopf boundary: the effective coupling should be such that it could bring the system into the multistable regime [9]. Here we keep the system near the Hopf boundary where mutual coupling can induce multistability (and as a result, robust chimera states). We focus on examining whether such states persist when the network structure is modified, especially the case when the topology creates dynamical frustration in the system. We first consider a ring topology with local and nonlocal interactions (with global coupling as a limiting case). For our multistable system with complex intermingled basins, this network enables dynamical frustration, and we study its effects on collective dynamics. We then extend our study to larger network sizes and also consider other complex network topologies, e.g., Watts-Strogatz small-world networks, Erdős-Rényi random graphs, and Barabási-Albert scale-free networks.

The spatial and temporal analysis of the oscillators in such ensemble shows intermittent dynamics: the trajectories of the oscillators may jump from one attractor to another, leading the system to show *intermittent chimeras*. We find that synchronization and desynchronization manifolds in the system, due to its complex structure, may push or pull oscillators' trajectories towards (or away from) a particular attractor, resulting in such intermittent behavior. The intermittent dynamics observed here can be classified as spatiotemporal intermittency since the coupled ensembles alter their dynamical states with respect to the time and the oscillatory units present in the network. We characterize this intermittent dynamics through local divergence plots [62,63]. Additionally, we numerically observe that the time interval of laminar phases scales as a power law. These results are verified for networks of different sizes, $N = 4$, 7, 10, and 300. We further consider various other complex network topologies, e.g., Watts-Strogatz small-world networks, Erdős-Rényi random graphs, and Barabási-Albert scale-free networks, and study the effects of network structure on chimera states. In all these networks, we observe spatiotemporal intermittent behavior due to the dynamical frustration in the networks with heterogeneous interactions (no mean-field-type interaction). This phenomenon becomes more prominent at relatively higher coupling strengths.

We would like to point out that similar intermittent behavior has been observed [10] in systems far from the Hopf bifurcation and interacting with symmetry breaking coupling (in x, y variables). Such a configuration leads to the observation of stable focus points, along with the solitary waves and metastable chimera states, which disappear for long evolution time. In contrast, since we are purposefully near the Hopf boundary, we do not observe stable focus points or solitary waves. Here robust chimera states observed in a globally coupled system become intermittent due to the dynamical frustration introduced through various nonmeanfield topologies. Further, we have used coupling through the z variable, which preserves the symmetry in x and y variables, and ensures that the observed dynamics do not appear due to the breaking of this symmetry. Our study also reaffirms the result that chaotic Lorenz attractor may actually exhibit chimera states [10], which was previously presumed not possible in the Lorenz system with quasihyperbolic attractors.

The organization of the paper is as follows. In the next Sec. II we consider Lorenz oscillators on a ring topology. We show multiple attractors observed in an example system of three oscillators when multistability is induced in such ensembles through the coupling. We discuss the dynamical scenarios that are observed on these attractors and how this may lead to an intermittent behavior including the occurrence of "intermittent chimera states." This phenomenon is examined by looking at the time evolution of the system and finite-time Lyapunov exponent. We analyze intermittent dynamics using local exponential divergence plots and interleaved time intervals. We also verify and discuss the generality of these results for different larger size networks. In Sec. III we further extend our study to networks of nonlocally coupled oscillator, and in Sec. IV for small-world, random graph, scale-free networks as well. This is followed by a summary and discussion in Sec. V.

II. LORENZ OSCILLATORS ON A RING

We consider a ring of $N = 3$ coupled Lorenz oscillators described mathematically by the following equations:

$$\dot{x}_i = \rho(y_i - x_i),$$
$$\dot{y}_i = \gamma x_i - y_i - x_i z_i,$$
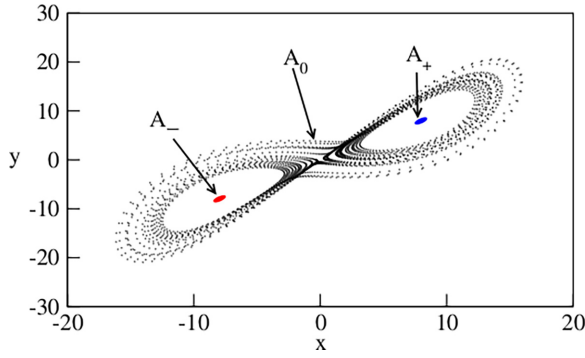$$\dot{z}_i = x_i y_i - \beta z_i + \varepsilon \Delta z_i, \tag{2}$$

FIG. 1. Multistable attractors A_-, A_+, A_0 observed in a coupled Lorenz oscillators [Eq. (2)] on a ring at coupling strength $\varepsilon = 0.02$.

where $\Delta z_i = z_{i-1} - 2z_i + z_{i+1}$, the index $i = 1, 2, \ldots, N$, and i is taken as module N. Oscillators are connected through z_i variables. Here ε represents the coupling strength, which is introduced in such a way that each node is connected to the left and to the right with equal strength. Since a Lorenz system is invariant under the transformation $(-x_i, -y_i, z_i) \to (x_i, y_i, z_i)$, coupling through z_i variables preserves the symmetry of the system in the x_i, y_i planes [58]. The Lorenz system has three steady states: $S_0 = (x_0^*, y_0^*, z_0^*) = (0, 0, 0)$ and $S_\pm = (x_\pm^*, y_\pm^*, z_\pm^*) = (\pm\sqrt{\beta(\gamma - 1)}, \pm\sqrt{\beta(\gamma - 1)}, \gamma - 1)$. For $\gamma < 1$, only one real stable equilibrium point S_0 exists and is stable. At $\gamma = 1$, the origin loses its stability, and the other two stable fixed points $S_\pm$ originate in the system. For parameter values $\gamma > 1$, all three equilibrium points exist. Note that $S_\pm$ remain stable for $1 < \gamma < \gamma_c$, where $\gamma_c = \frac{\rho(\rho + \beta + 3)}{\rho - \beta - 1} \approx 24.74$ is the critical parameter. At $\gamma = \gamma_c$, the fixed points $S_\pm$ collide with an unstable limit cycle (which exist between $13.926 < \gamma < \gamma_c$) and become unstable through a subcritical Hopf bifurcation. The system exhibits a very rich and interesting dynamics including reverse period-doubling bifurcations, periodic windows, transient chaos, and chaos [2,64]. In this work, the parameter values are $\rho = 10$, $\beta = 8/3$, and $\gamma = 24.76 = \gamma_c + 0.02$ (just above the Hopf bifurcation point γ_c), taken such that the fixed points of the isolated oscillators $S_\pm$ [2,64] are unstable and the dynamics of each of the uncoupled oscillator is chaotic.

In the absence of coupling, the oscillators in this ensemble settle into the well-known Lorenz chaotic attractor A_0. In the coupled system, however, one observes two new symmetric-stable attractors denoted by A_+ and A_- along with the typical attractor A_0 (see Fig. 1). It is observed that the oscillators settling into attractors A_+ and A_- show synchronized behavior while the motion on A_0 is desynchronized [9]. These distinct synchronization properties of the attractors give rise to induced chimera states through mutistability. In the system of N oscillators, the dynamics can take place in three possible manifolds. A fully desynchronized motion on A_0 takes place in a $3N$-dimensional desynchronized manifold $\mathcal{M}_d$, whereas, when synchronization is established in the system, the condition $x_i = x_j, y_i = y_j, z_i = z_j$, for all i, j is satisfied. These $(3N - 3)$ constraints on the motion reduce the dimension of the system, with the dynamics taking place on a three-dimensional subspace, the synchronization manifold, $\mathcal{M}_s$. Similarly, fulfillment of the antisynchronization condition,
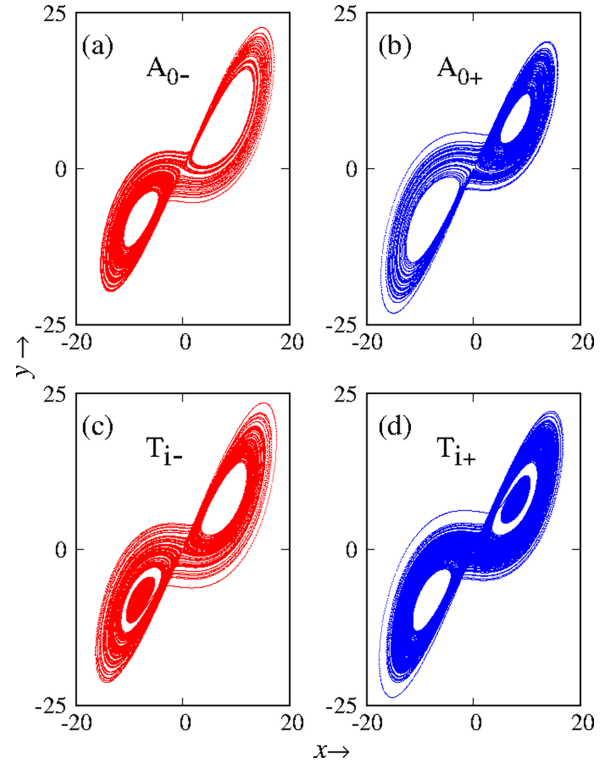

FIG. 2. Different dynamical behavior observed in the system. At $\varepsilon = 0.05$, the biased motion is shown in (a) and (b), where the trajectory remains in one of the lobes while moving on attractor A_0, denoted by A_{0+} and A_{0-}. For higher coupling ($\varepsilon = 0.10$), the trajectories on an attractor can also jump to another attractor as shown in (c) and (d), denoted by trajectories T_{i+} and T_{i-}.

$x_i = -x_j, y_i = -y_j, z_i = z_j$ represents a motion on antisynchronization manifold $\mathcal{M}_a$. Dimensions of these subspaces depend upon the number of constraints, i.e., the number of synchronized and antisynchronized oscillators. Coexistence of a desynchronized manifold with either one or both of these other manifolds implies the existence of chimeric states.

The typical attractors observed in the system of a coupled Lorenz system are shown in Fig. 1. Depending on the initial condition, the oscillators in the ensemble can end up in any of these attractors. As mentioned before, these coexisting attractors are responsible for a system's chimeric behavior due to their distinct synchronization properties: oscillators settling into attractor A_0 show desynchronized behavior, but the ones which asymptote to A_+ and A_- show synchrony while being in antisynchrony with each other. Besides these attractors, additional dynamical motions which we observe on a ring of coupled Lorenz oscillators are shown in Fig. 2. For example, a biased motion in shown in Figs. 2(a) and 2(b), where the trajectory spends more time in one of the wings of the chaotic Lorenz attractor A_0. Further, we observe that oscillators may not be contained within one attractor and can jump from one attractor to another as shown in Figs. 2(c) and 2(d), where the trajectory jumps between attractors, represented by trajectories T_i.

Coupled Lorenz oscillators with multistable behavior have complex basin structures [6,61], giving rise to the chimera states [9] in such systems. Similar to globally coupled
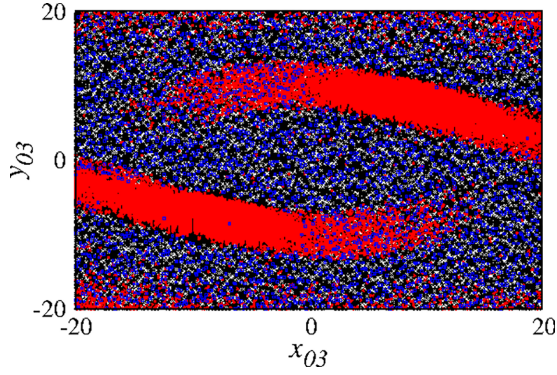
FIG. 3. Basin of attraction of the system of three coupled Lorenz oscillators on a ring at coupling strengths $\varepsilon = 0.028$. Basins are calculated for initial conditions in x_3 and y_3 variables, i.e., x_{03}, y_{03} space in the interval $[-20, 20]$. Initial values of $x_1, y_1, z_1, x_2, y_2, z_2, z_3$ are fixed, i.e., $x_{01} = x_{02} = y_{01} = y_{02} = z_{01} = z_{02} = z_{03} = 1$. The initial conditions evolving towards different dynamics are represented by white, blue (dark gray), red (light gray), and black regions (see text for details).

oscillators, the basin of attraction of this system also shows riddled behavior: trajectories starting with infinitesimally close initial conditions have a nonzero probability of ending up into different attractors. The complexity of the basin implies that the manifolds containing oscillator trajectories are also very complex. In Fig. 3 we plot the basin of attraction of the system of three coupled oscillators at $\varepsilon = 0.028$. Here white regions are where all the oscillators evolve to the A_0 attractor, and the dynamical state can be represented as (A_0, A_0, A_0). Red (light gray) and blue (dark gray) regions correspond to the collective states $(A_0, A_\pm, A_\pm)$ and $(A_0, A_0, A_\pm)$, respectively. The black region indicates a collective state $T_{i\pm}$ where at least one oscillator has intermittent dynamics and the other oscillators may evolve to any of the coexisting attractors.

The intermittent dynamics of the oscillators observed for the coupled system at $\varepsilon = 0.03$ is shown in Fig. 4. The first oscillator spends a large amount of time in a A_0-type state, but then jumps to A_+ attractor as shown in Figs. 4(a) and 4(b). Dynamics of the second oscillator is initially on A_- followed by A_0 and jumps to an A_+-type attractor. This is shown in Figs. 4(c) and 4(d). As shown in Figs. 4(e) and 4(f), the dynamics of the third oscillator is on the A_- attractor before jumping to A_0. For all these cases system may again jump to another attractors when it is evolved further. Time series plots of the x variable are plotted in Fig. 5 to show more prominent intermittent dynamics at higher coupling strengths. The hopping between different dynamical states becomes fast as the value of coupling strength is increased [33] as shown in Figs. 5(b)–5(d).

This complex intermittent behavior can be verified by plotting the distribution of finite-time Lyapunov exponents λ. With increasing strength of coupling, we examine finite-time Lyapunov exponents calculated for relatively small time-intervals taken from a long trajectory, and plot its probability distribution function (PDF) with coupling strength in Fig. 6. Finite-time Lyapunov exponents provide information about average convergence or divergence rate of two nearby trajectories within the attractor for a given time window. Since
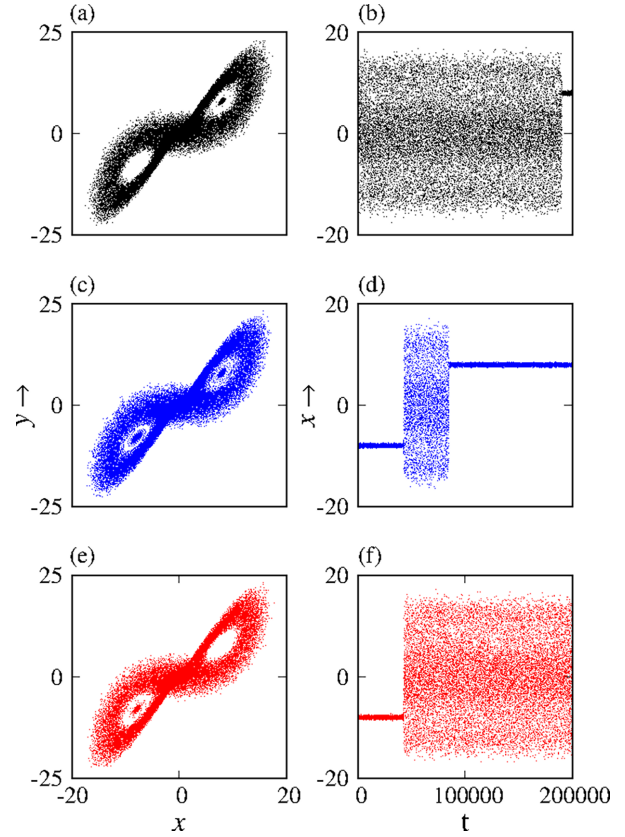

FIG. 4. Plots for intermittent dynamics (left panel) and their corresponding time series (right panel). In (a) an oscillator spends large amount of time in the A_0 attractor but jumps to A_+. (b) Representation of their corresponding time series. In (c) and (d), we observe two jumps from initial attractor A_- to A_0 and then to A_+. A jump from smaller attractor A_- to bigger attractor A_0 is shown in (e) and (f).

here the trajectories may switch between different attractors, two peaks are observed due to the different convergence (or divergence) rate on those attractors. In Ref. [36] it was shown that in case of intermittency, the PDF of the local LE is a combination of a normal density and a stretch exponential tail. For the case of an uncoupled map, authors have shown that for intermittency, the local LE has a Gaussian distribution centered at different values and a stretched exponential tail that interpolates between the two. The distribution of the exponents indicates that the trajectories in some time windows can fall apart or can come close while moving within an attractor. Two peaks in the PDF correspond to the states between which the intermittent dynamics takes place. In the present case, the PDFs of the local LE are plotted in Fig. 6(a) for different values of ε. As shown, the PDF consists of two peaks P_1 and P_2, which clearly indicates the presence of two distinct behaviors. To understand the interpolation between the two peaks (P_1 and P_2) [36], we plot the PDF in Fig. 6(b) for two values of ε and observe that it is a straight line indicative of an exponential behavior.

We characterize these intermittent states by using local exponential divergence plots proposed by Gao et al. [62,63] as follows. These plots are used to characterize complex motions and can be applied directly to the experimental
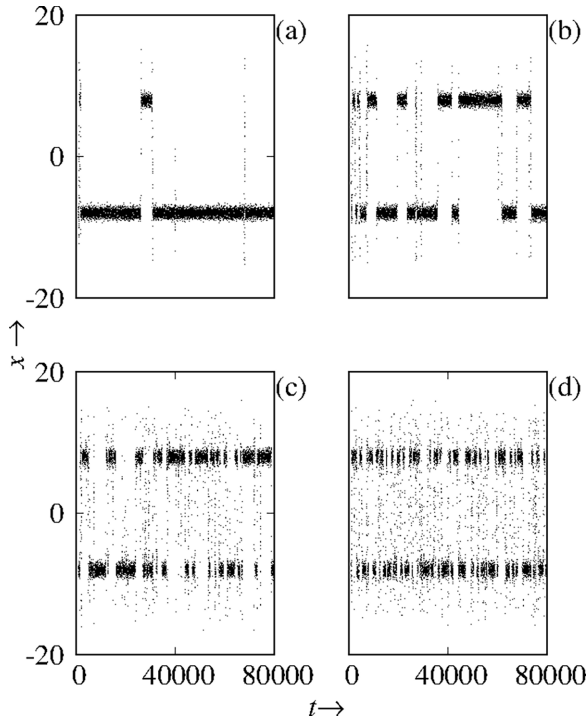
FIG. 5. Effect on intermittent behavior for different coupling strength values. Time series of variable x is plotted to see intermittent dynamics at (a) $\varepsilon = 0.08$, (b) $\varepsilon = 0.09$, (c) $\varepsilon = 0.11$, and (d) $\varepsilon = 0.12$.

time series. Here we outline the procedure to calculate this exponent for the time series given by $x(1), x(2), \ldots, x(N)$ normalized to the unit interval [0,1]. We then make use of time-delay-embedding [65,66] procedure to construct vectors of the form $X_i = [x(i), x(i + L), \ldots, x(i + (m - 1)L)]$, where m is the embedding dimension and L is the delay time to be chosen such that the optimization criteria are satisfied. The time-dependent exponent $\Lambda(k)$ is defined as

$$\Lambda(k) = \left\langle \ln \left(\frac{||X_{i+k} - X_{j+k}||}{||X_i - X_j||} \right) \right\rangle, \quad (3)$$

where $d \leqslant ||X_i - X_j|| \leqslant d + \Delta d$, with d and Δd being small distances and $||.||$ denotes the Euclidean norm. Angular brackets denote the ensemble average over all possible pairs (X_i, X_j) and k is the evolution time. Computation is carried out for a series of shells $(d, d + \Delta d)$. For a purely chaotic signal, the $\Lambda(k)$ curve first increases linearly and then flattens. The linear regime for different shells collapses to form a common envelope. As shown in Fig. 7, we plot the $\Lambda(k)$ versus k curve for the intermittent dynamics at $\varepsilon = 0.09$, and we note that the common envelope is well defined, indicating that the dynamics is chaotic.

We observe that for the coupling range $0.011 < \varepsilon < 0.17$ trajectories display intermittent synchronization or intermittent antisynchronization. To avoid the effects of numerical artifacts on properties of intermittency [67], we have performed simulations with double precision. Figure 8(a) shows spatiotemporal intermittency consisting with intermittent synchrony (antisynchronized) and incoherent dynamics, i.e., the intermittent chimera states. Here intermittent synchrony (or
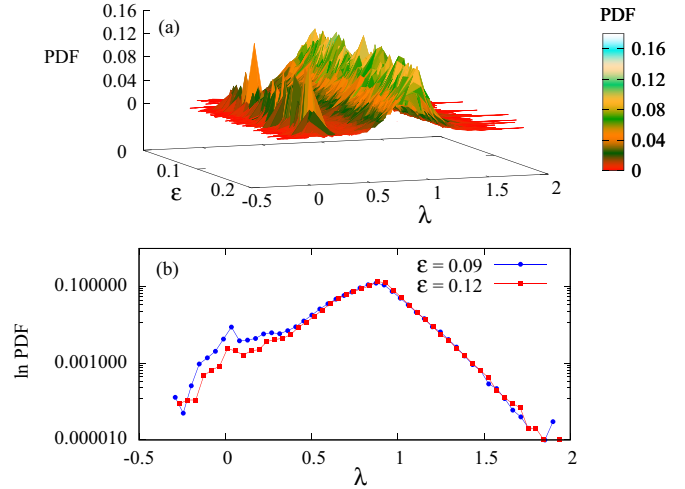

FIG. 6. Distributions (PDFs) of finite-time Lyapunov exponents λ are plotted with coupling strength ε. Two visible peaks correspond to two different attractors and indicate that the trajectory may switch between two dynamical behaviors in time. In (b) we plot the logarithm of the PDF showing that the two peaks can be interpolated through a straight line in the semilog graph. These exponents are calculated along a very long trajectory which is divided into segments of equal finite-time lengths $t = 10$. The finite-time Lyapunov exponent is then calculated for each segment.

antisynchrony) refers to the case when two or more oscillators are synchronized (or antisynchronized) for some interval of their evolution time, and for the remaining interval, the oscillators are not in synchrony. As shown in Fig. 8(a) at $\varepsilon = 0.11$, oscillator 1 shows intermittent synchrony with oscillator 2, for which the time series is plotted in Fig. 8(b). Intermittent synchrony is evident from the time series of the difference of their x variables, namely, $x_1 - x_2$ in Fig. 8(d). Similarly, antisynchronization is observed between oscillators 1 and 3 for which the time series is plotted in Fig. 8(c). The sum of these variables, $x_1 + x_3$ is plotted in Fig. 8(e), which shows intervals of antisynchrony and desynchrony. We explore the nature of
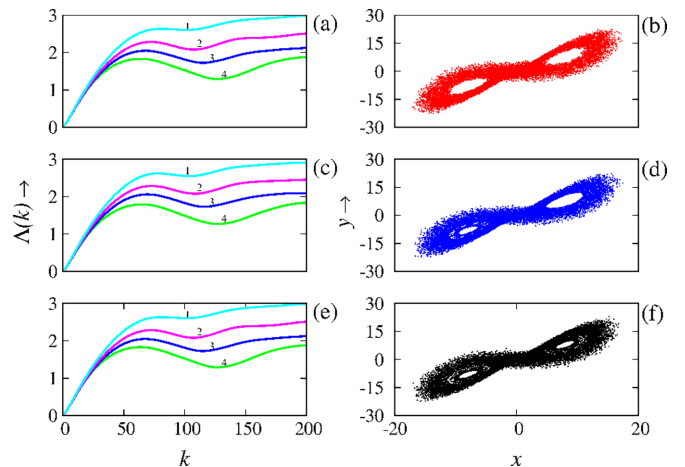

FIG. 7. $\Lambda(k)$ curve for the time series of an intermittent attractor obtained at $\varepsilon = 0.09$. The numbers 1 to 4 correspond to shells defined by $(2^{-(i+1)/2}, 2^{-i/2})$ with $i = 9$ to 12.
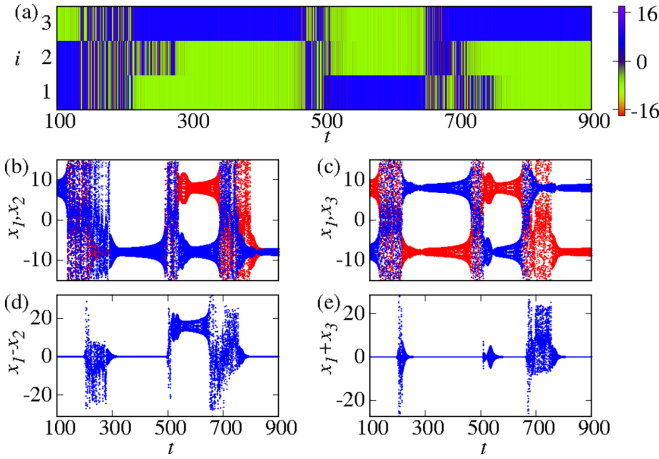
FIG. 8. Spatiotemporal intermittent dynamics consisting of intermittent synchrony (or antisynchrony) and incoherent states i.e., an intermittent chimera shown for the system of $N = 3$ coupled Lorenz oscillators [Eq. (2)] on a ring with coupling strength $\varepsilon = 0.11$. The space-time plot with variable x for all oscillators is shown in (a). Time series of the oscillators are compared by plotting variables x_1, x_2 and x_1, x_3 in (b) and (c), respectively. In subplots (d) and (e) we plot the difference $x_1 - x_2$ and sum $x_1 + x_3$, respectively to show synchronization and antisynchronization between the oscillators.

intermittent synchronization and desynchronization following the procedure by Baker *et al.* [67]. We store the interleaved intervals of synchronized (antisynchronized) dynamics and sort them according to the duration τ of the individual segments. The distribution of τ turns out to be a power law with an exponent $\zeta = -2.23$ (see Fig. 9) as expected for the case of intermittent dynamics [27]. Further, we applied Kolomogorov–Samirnov (KS) test on our data to calculate the p value after performing a statistical t test. Using SPSS and Python simulation, we observed a p value $= 0.4999$, and since the p value is greater than the critical parameter ($p > 0.1$), this
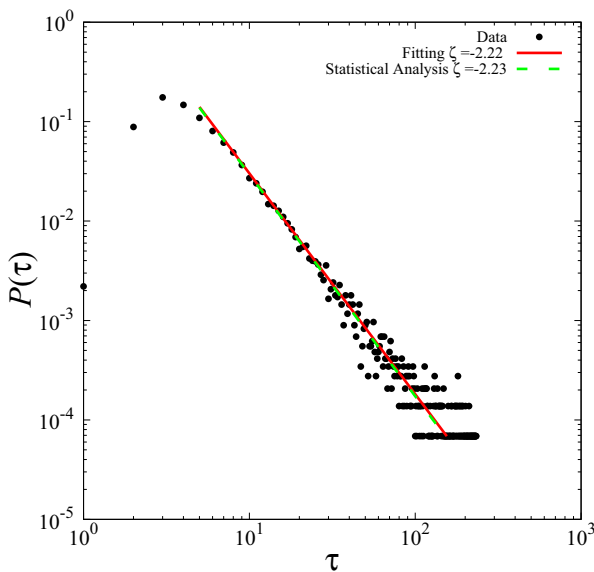

FIG. 9. Power-law behavior of the distribution of interleaved intervals τ at $\varepsilon = 0.12$.
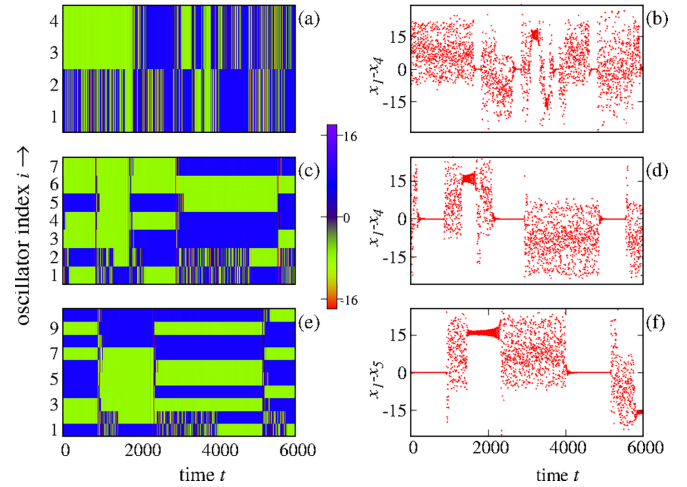

FIG. 10. Spatiotemporal intermittent dynamics in the coupled Lorenz oscillator for different network sizes. The results for $N = 4$ (a, b), 7 (c, d), and 10(e, f) are plotted in each row at coupling strength $\varepsilon = 0.12$. The space-time plots and difference variables indicating synchronization are plotted on the left and right panel, respectively. The results confirm the existence of intermittent chimera states for larger networks.

confirms power-law behavior of the distribution of interleaved intervals in our system [68].

We also observed such intermittent behavior for different network sizes. The results for $N = 4, 7, 10$ oscillators on a ring are shown in Fig. 10. The left panel of the figure shows the space-time plot. The time series of the difference variable $x_i - x_j$ are plotted in the right panel. These results verify the existence of intermittent synchrony and antisynchrony in larger systems. The intermittent behavior of the oscillator appears due to the frustration introduced by neighboring oscillators with different dynamical properties: we found that such intermittent synchrony and antisynchrony is not observed for globally coupled oscillators. An oscillator in one attractor hops between different attractors depending upon the forcing from its neighbors.

The emergence of intermittent chimera states observed in our system can be explained as follows. In a ring topology considered here, the dynamics of an oscillators depends on the signals received from its left and right neighbors. When the neighboring oscillators asymptote to different attractors, the oscillator may show frustrated dynamics and be pulled towards another manifold. We find, due to such frustration and the complex manifold structures, that oscillators' trajectories may show biased motion and may not even be contained within one attractor. For example, the oscillators on one attractor may stay in the vicinity of another attractor for a relatively longer time, resulting in a biased motion shown in Figs. 2(a) and 2(b). Further, the trajectories may also jump from one to another attractor [see Figs. 2(c) and 2(d)]. With increasing coupling strength, the frustration get stronger, making these jumps more frequent (see Fig. 5). This gives rise to intermittent dynamics observed in the system. Such intermittent jumps between different attractors also change the synchronized property of the system, resulting in the system showing *intermittent chimera* states.
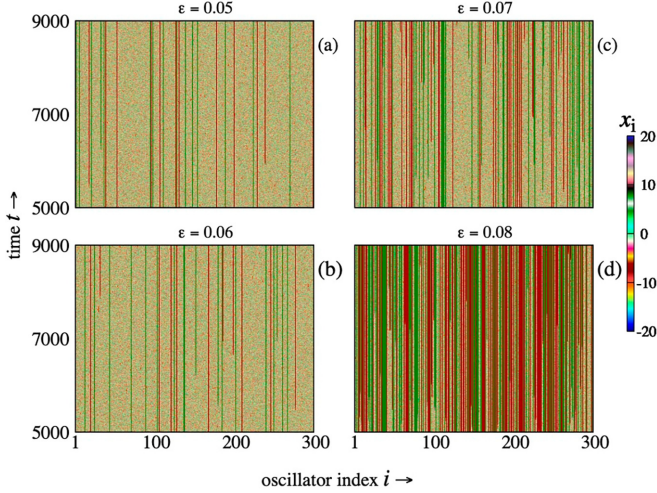
FIG. 11. Time evolution of space variables x_i for a system of $N = 300$ locally coupled oscillators [Eq. (4)] at different coupling strengths ($\varepsilon = 0.05$, 0.06, 0.07, and 0.08). We observe intermittent behavior, with the jumps becoming more frequent with increasing coupling strength.

III. INTERMITTENCY IN A NETWORK OF NONLOCALLY COUPLED OSCILLATORS

To substantiate our findings for smaller values of N, we consider an ensemble of nonlocally coupled oscillators for which the dynamical equations are given by

$$\dot{x}_i = \rho(y_i - x_i),$$
$$\dot{y}_i = \gamma x_i - y_i - x_i z_i,$$
$$\dot{z}_i = x_i y_i - \beta z_i + \frac{\varepsilon}{2p} \sum_{j=(i-p)}^{(i+p)} (z_j - z_i). \qquad (4)$$

Each oscillator in the network is connected symmetrically with $2p$ nearest neighbors (p to its left and p to its right) with coupling strength ε. The coupling radius of the network is $r = p/N$ [39]. For $p = 1$, oscillators are coupled only to one of its nearest neighbor on both sides (ring topology), and the coupling scenario is referred to as the local with coupling radius $r = 1/N$. For global coupling, all the oscillators are connected to each other, i.e., $p = (N-1)/2$ or $\approx N/2$ and coupling radius $r = (N-1)/2N \approx 0.5$ depending on whether N is odd or even. The value of r between these limits refers to nonlocally coupled scenarios [69,70].

Dynamics for the locally coupled oscillators ($p = 1$) is shown in Fig. 11 at different coupling strengths. Here we plot time evolution of the space variables x_i for a system of $N = 300$ oscillators and observe intermittent chimera states in the system. This dynamics gets more prominent as the coupling strength ε is increased (see Fig. 11). However, the intermittent behavior disappears for very strong coupling strengths, and we observe synchronized cluster states where the dynamics evolves towards either the A_+ or A_- attractor.

The results for nonlocal coupling scenarios with different coupling radii $r = 0.1$, 0.2, and 0.3 is plotted in different columns of Figs. 12(a)–12(i). The limiting case of a global coupling scenario ($r = 0.5$, $p = 150$) is shown in
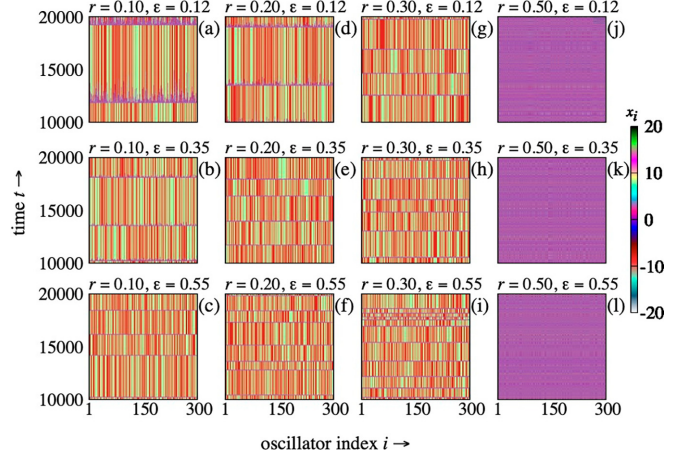

FIG. 12. Time evolution of space variables x_i for a system of $N = 300$ coupled oscillators [Eq. (4)] at different coupling strengths and coupling radii. The results for nonlocal coupling with coupling radii $r = 0.1$ ($p = 30$), $r = 0.2$ ($p = 60$), and $r = 0.3$ ($p = 90$) are shown in the first, second, and third columns, respectively. The last (fourth) column shows the results for global coupling with $r = 0.5$ ($p = 150$). The top ($\varepsilon = 0.12$), middle $\varepsilon = 0.35$, and last $\varepsilon = 0.55$ rows show behavior for different coupling values. Intermittent behavior is observed for nonlocal coupling scenarios where the intermittent jumps become more frequent with increasing coupling strength. For globally coupled oscillators shown in last column, this intermittent behavior is not observed.

the last column [Figs. 12(j)–12(l)]. For each r, we plot the time evolution of the variable x at different coupling strengths. For such nonlocal coupling scenarios, we again observed intermittent chimera states. We note that at smaller values of coupling strengths, an oscillator in the network spends a relatively longer time on a given attractor; i.e., hopping between attractors is rare. Further, as the value of a coupling parameter is increased, hopping between the attractors becomes very frequent. We also note that when coupling radius is increased to an optimal value, i.e., for global coupling ($r = 0.5$, $p = 150$), such intermittent behavior is not observed, as shown in Figs. 12(j)–12(l). In this case, system dynamics evolves towards the A_0-type attractor, and their collective states are either synchronized or antiphase synchronized as shown in Fig. 13. This indicates that the intermittent behavior emerges as a result of frustration introduced by local and nonlocal coupling scenarios.

IV. DYNAMICS ON OTHER COMPLEX NETWORKS

In this section we extend our analysis to the small-world, random, and scale-free networks to see if the intermittent dynamics can be observed in more general and complex settings. The equations governing the dynamics of the oscillators in these networks are given by

$$\dot{x}_i = \rho(y_i - x_i),$$
$$\dot{y}_i = \gamma x_i - y_i - x_i z_i,$$
$$\dot{z}_i = x_i y_i - \beta z_i + \varepsilon \sum_{j=1}^{N} A_{ij}(z_j - z_i), \qquad (5)$$
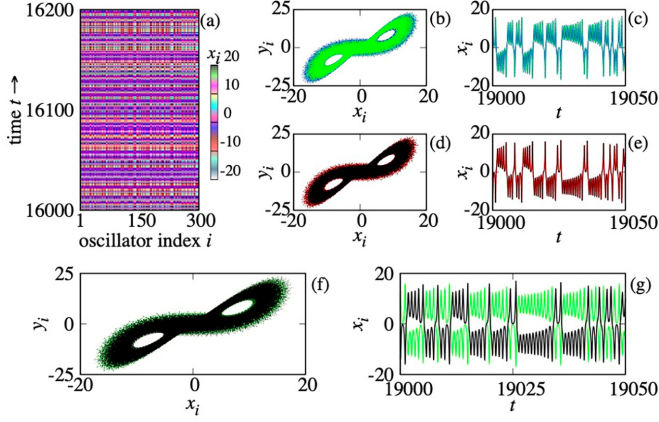
FIG. 13. (a) Zoomed-in behavior for global coupling scenario [Figs. 12(j)–12(l)]. Two randomly selected attractors from synchronized groups are plotted in (b) and (d), along with the corresponding time series in (c) and (e), respectively. Panel (f) shows the attractors from the antisynchronized group with the corresponding time series shown in (g).

where $\boldsymbol{A} = \{A_{ij}\}$ is the adjacency matrix that describes the connection topology of the network. The matrix elements $A_{ij} = A_{ji} = 1$ if there is a link from i to j and 0 otherwise. In the following subsections, we consider various complex networks, obtain corresponding adjacency matrices $\boldsymbol{A}$ using briefly described standard algorithms for generating such topologies, and investigate the emergence of the intermittent chimeric dynamics in these networks.

A. Intermittent behavior in small-world networks

The matrix elements $\{A_{ij}\}$ in Eq. (5) for generating small-world networks is given by the Watts-Strogatz (WS) algorithm [71]. This model is parameterized by a "rewiring probability" denoted by δ and describes networks that simultaneously account for both clustering and small-world properties. For $\delta = 0$ (no rewiring), this model gives a regular ring lattice with each node coupled to its $2p$ nearest neighbors, and for $\delta = 1$ (all connections randomly rewired), it provides a random graph.

The collective behavior for such a WS network with $N = 300$ and $p = 30$ at different rewiring probabilities δ is depicted in Fig. 14. For each selected configuration (δ value), we analyze the collective behavior of the oscillators at different coupling values. As expected, similar to previous observations, spatiotemporal intermittency increases in the network as a function of coupling strength ε (different rows in Fig. 14). Furthermore, we note that there are no significant changes in the intermittent dynamics as rewiring probability δ is increased; see the first row in Fig. 14. Note that, by increasing δ, we are not adding new connections in the network but rewiring the existing ones only. This rewiring doesn't seem to cause much change in the overall frustration an oscillator experiences in the network. As a result, we observe only minor changes in the intermittent dynamics as the rewiring probability is increased (first three columns). However, when rewiring probability is one (corresponding to an entirely random network), we do not observe strong intermittent behavior
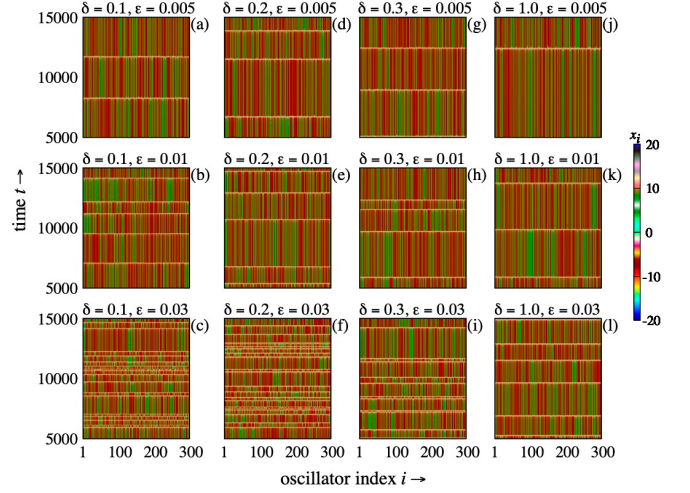

FIG. 14. For small-world networks with $N = 300$ and $p = 30$ (p denotes node degree of the initial regular graph), we show the time evolution of space variables x_i at different rewiring probabilities δ and coupling strengths ε. Results for $\delta = 0.1$, 0.2, 0.3, and 1.0 are shown in first, second, third, and fourth columns, respectively. Note that the fourth column represents limiting case with completely rewired connections, i.e., a random network. Plots for different couplings $\varepsilon = 0.005$, 0.01, and 0.03 are shown in the top, middle, and bottom rows.

even at higher coupling strengths; see the fourth column for $\delta = 1.0$ in Fig. 14. This observation can be attributed to the fact that the networks with more random configurations and high node degree are topologically less heterogeneous: the majority of the oscillators are subjected to similar random interactions. For most of the oscillators, this makes one of the attractors a more likely asymptotic state reducing the frustration effects in the network, especially at lower couplings. We can clearly verify this effect with the system showing weak intermittency even for higher coupling strengths (see Fig. 14, last column).

As mentioned, here we create small world (WS) networks by rewiring a fraction of the connections δ ($0 < \delta < 1$) of a regular graph with p nearest-neighbor coupling. In Fig. 15 we analyze system dynamics of WS networks by rewiring different initial regular graphs with different node degrees, i.e., different p values: we plot the time evolution of x_i variables for different initial configurations $p = 10, 20, 40$, and 100 at a fixed rewiring probability $\delta = 0.4$. Again, we clearly see that the intermittent behavior is more prominent for higher coupling strengths. Note that for larger p values, the network configuration tends towards global (all-to-all) type interactions. Then one can safely argue that the nodes in such networks are subjected to averaged-out influence of large number of other nodes. This scenario results in less frustration and correspondingly less frequent hopping between different dynamical states. At very large p and ε values [for example, see Figs. 15(i), 15(k), and 15(l)], the frustration effects disappear, and therefore, so does the intermittent behavior. For this case, we observe that the network shows either synchronized or antisynchronized behavior (similar to behavior shown in Fig. 13).
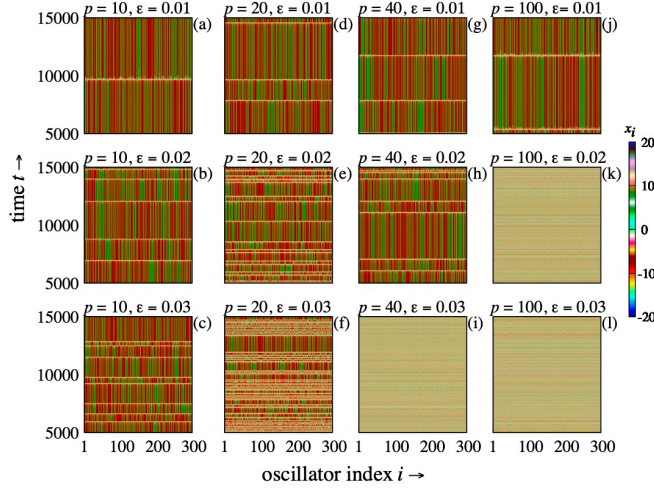
FIG. 15. For small-world networks with $N = 300$ and rewiring probability $\delta = 0.4$, we show the time evolution of space variables x_i for different coupling strengths ε and different initial networks (regular graphs) with p-nearest-neighbor coupling. Results for $p = 10$, $p = 20$, $p = 40$, and $p = 100$ are shown in first, second, third, and fourth columns, respectively. Plots for different coupling strength $\varepsilon = 0.01$, $\varepsilon = 0.02$ and $\varepsilon = 0.03$ are shown in first, second, and third rows. More frequent intermittent jumps are observed with higher couplings. However, intermittent jumps get suppressed for highly connected networks (higher p values), especially at higher coupling strengths.

B. Intermittent behavior in random and scale-free networks

In this subsection we present the results for a random and a scale-free graphs with $N = 300$ nodes. The random network is generated using the Erdős and Rényi (ER) graph model [72]. Every edge in this network has a fixed equal probability $\eta \in [0, 1]$ of being in the graph. As the value of η increases from 0 to 1 the probability of including more edges in the graph also increases. Here the probability that a given node has a degree k is given by the binomial distribution $P(k) = \binom{N}{k} \eta^k (1 - \eta)^{N-1-k}$, which, for large N and small η, can be approximated by the Poisson distribution $P(k) = \frac{\langle K \rangle^k e^{-\langle K \rangle}}{k!}$ with $\langle K \rangle = \eta(N - 1)$.

We also analyze scale-free networks here, for which we use the Barabási-Albert (BA) model [73]: we grow the network by sequentially adding new nodes with preferential attachments rule. A new node with m open edges is added to the existing network at each time step with preferential attachment, i.e., the probability η_i of a new node getting connected to the existing node i is proportional to its degree k_i, $\eta_i = \frac{k_i}{\sum_j k_j}$.

The results for such random and scale-free networks are shown in Figs. 16 and 17, respectively. In both cases we observe spatiotemporal intermittency. As expected, the dynamics becomes more prominent for higher coupling strengths. Also, a moderate increase in average degree $\langle K \rangle$ and coupling strength ε leads to more frequent jumps between the states [Figs. 16(a)–16(f)]. However, for large couplings, and when the structure is modified to be more like globally interacting configurations (large average degree), the intermittent dynamics gets suppressed as seen in Fig. 16(i). Similar results are observed for scale-free networks shown in Fig. 17,
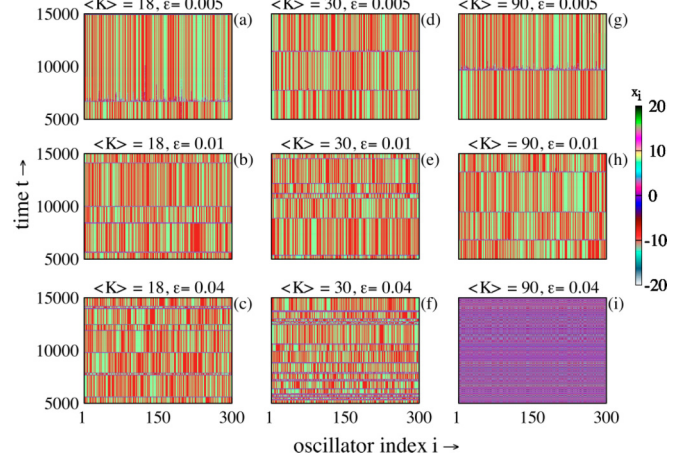

FIG. 16. Time evolution of space variables x_i for a random network of $N = 300$ oscillators [Eq. (5)]. The results for different average degree $\langle K \rangle = 18$, $\langle K \rangle = 30$, and $\langle K \rangle = 90$, respectively, are shown in different columns. Different rows represent results for different coupling strength $\varepsilon = 0.005$, $\varepsilon = 0.01$, and $\varepsilon = 0.04$, respectively. The system exhibits spatiotemporal intermittent behavior in (a)–(h), and synchronized and antisynchronized dynamics (see Fig. 13) for higher $\langle K \rangle$ and ε values in (i).

where we generate different scale-free networks by sequentially adding new nodes with different open connections $m = 3, 5, 10$, and 15. These networks have a few highly connected nodes, and the average connectivity increases with increasing m values. Similar effects on intermittent behavior are observed as a function of coupling strength and m in this case as well.

These results indicate that intermittent dynamics can be observed due to the dynamical frustrations arising in variety of networks including ring, nonlocal, small-world, random,
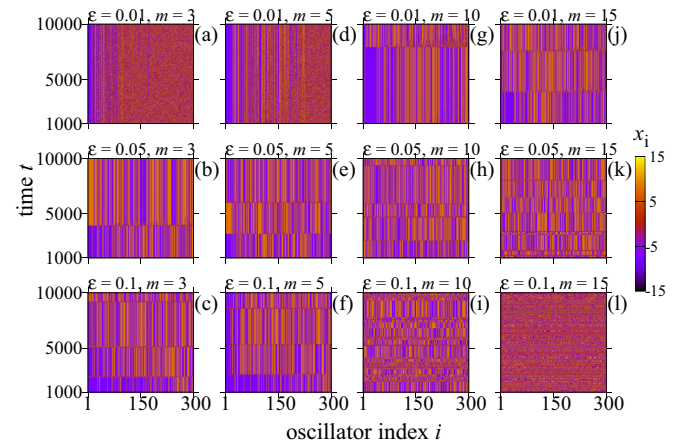

FIG. 17. Time evolution of the variable x_i is plotted for a scale-free network with $N = 300$ oscillators [Eq. (5)]. Different open connections m and coupling parameters are shown in columns and rows, respectively. The results for $m = 3$, $m = 5$, $m = 10$, and $m = 15$ are shown in different columns. In the rows, respectively, indicate coupling values $\varepsilon = 0.01$, $\varepsilon = 0.05$, and $\varepsilon = 0.1$. The network exhibits spatiotemporal intermittent nature, which is suppressed at strong coupling in network with highly connected clusters (i) $m = 15$ and $\varepsilon = 0.1$.

and scale-free configurations. This behavior becomes more prominent with higher coupling strengths and gets suppressed if the network configuration supports mean-field-type interaction, for example, for strongly interacting highly connected networks.

V. SUMMARY

In the present work, we study collective behavior of coupled Lorenz oscillators near the Hopf boundary. This system shows multistable behavior where the coexisting attractors have different dynamical properties. Due to such multistability, such systems are known to exhibit chimeric behavior in a globally coupled setting. Here our motivation is to understand the effect of topology on such chimeric behavior—specifically the effect of frustration, which is introduced in the system using ring topology with $2p$-nearest-neighbors interactions and small-world, random, and scale-free network topologies. We find that due to the introduction of frustration in this multistable system, the dynamics becomes intermittent. As a result of this intermittent behavior, the oscillators hop between synchronized and desynchronized motions, and we observe intermittent chimera states in the system. We also observe that this intermittent dynamics becomes more prominent as the coupling strength is increased and when the network is topologically heterogeneous and supports frustration effects. This suggests that the hopping of the oscillators depends on the interactions with its neighbors, generating strong frustrations responsible for such behavior.

Using an example of $N = 3$ oscillators on a ring, we show how the dynamics may exhibit biased behavior, namely, when the trajectory remains in the vicinity of another attractor for a longer time or exhibit intermittent jumps to other attractors. This intermittent behavior makes resulting dynamics of larger ensembles even richer where multiple oscillators may hop intermittently between different attractors. In such an oscillator ensemble, the trajectories of the oscillators lie in a complex subspaces, namely, synchronized, antisynchronized, and desynchronized manifolds. The oscillators from the network may split or merge from the synchronized subpopulation depending on the synchronization property of the attractor towards which it intermittently goes. As a result of such hoping, oscillators may switch manifolds, and the phenomenon of intermittent chimeras is observed in the system. The complexity of the coexisting attractors can be further explored by plotting the local exponential divergence plots, which can be applied directly to the time series data. It is evident from the divergence plots that the coexisting intermittent attractors are chaotic in nature. These attractors are responsible for the occurrence of intermittent synchronization and antisynchronization for which the locking times show a power-law decay.

Note that the chimera state is a spatiotemporal phenomenon where spatially distributed oscillators show two distinct temporal dynamics: coherent and incoherent motion.

The phenomenon of intermittency refers to the temporal alteration (slippage) between different dynamical states. In our system, we find both: first, the different oscillators of the ensemble may asymptote towards different attractors in phase space leading to the chimeric behavior, and second, there can be intermittent jumps between synchronized and incoherent attractors modifying a system's chimeric properties. These jumps result in the emergence of intermittent chimeras where we find coexistence of intermittent-synchrony and incoherent states.

The intermittent dynamics we observe here is due to the frustration created by its neighbors. This happens when the trajectories of neighboring oscillators lie in different manifolds, i.e., they are moving on different attractors. The connected oscillator is entrained towards both of these motions creating the frustration, which consequently leads to the hopping between different manifolds and therefore intermittent dynamics shown by the oscillator. This condition is readily fulfilled in the ring topology, especially for regular ones (local and nonlocal coupling strategies). However, for the globally coupled oscillators such intermittent behavior is not observed since all oscillators feel an averaged mean field effect due to all-to-all coupling. In highly connected networks where the oscillators are subjected to less frustration, such intermittent dynamics gets suppressed. These results are verified for Watts-Strogatz small-world networks, Erdős-Réyni random graphs, and Barabási-Albert scale-free networks. This indicates that such behavior is quite general and can be used to understand collective dynamics of various other network topologies as well.

Intermittent chimera states have been observed in experimental systems with or without multistable dynamics, for example, waveguide resonators [74], electrochemical systems [75], and mechanical rotators [76]. In addition to these time-continuous systems, the existence of such states was recently reported in discrete-time systems of coupled map lattices [77]. It is an open question whether such states can be observed in cellular automata as well. Chimera states have already been observed in various experimental setups including Josephson junction arrays and coupled lasers. Therefore, it would be interesting to explore the intermittent behavior of multistability-induced chimera states in such systems.

[1] E. N. Lorenz, J. Atmos. Sci. **20**, 130 (1963).

[2] C. Sparrow, *The Lorenz Equations: Bifurcation, Chaos, and Strange Attractors* (Springer, New York, 1982).

[3] L. M. Pecora and T. L. Carroll, Phys. Rev. Lett. **64**, 821 (1990).

[4] L. M. Pecora, T. L. Carroll, G. A. Johnson, and D. J. Mar, Chaos **7**, 520 (1997).

[5] L. M. Pecora and T. L. Carroll, Chaos **25**, 097611 (2015).

[6] S. Camargo, R. L. Viana, and C. Anteneodo, Phys. Rev. E **85**, 036207 (2012).

[7] K. Konishi, Phys. Rev. E **70**, 066201(R) (2004).

[8] R. Karnatak, R. Ramaswamy, and A. Prasad, Phys. Rev. E **76**, 035201(R) (2007).

[9] S. R. Ujjwal, N. Punetha, A. Prasad, and R. Ramaswamy, Phys. Rev. E **95**, 032203 (2017).

[10] I. A. Shepelev, G. I. Strelkova, and V. S. Anishchenko, Chaos **28**, 063119 (2018).

[11] G. Xiao, W. Liu, Y. Lan, and J. Xiao, Nonlinear Dyn. **93**, 1047 (2018).

[12] A. A. Koronovskii, O. I. Moskalenko, A. A. Pivovarov, V. A. Khanadeev, A. E. Hramov, and A. N. Pisarchik, Phys. Rev. E **102**, 012205 (2020).

[13] Y. C. Lai and C. Grebogi, Phys. Rev. E **47**, 2357 (1993).

[14] J. G. Restrepo, E. Ott, and B. R. Hunt, Phys. Rev. E **71**, 036151 (2005).

[15] R. Karnatak, R. Ramaswamy, and A. Prasad, Chaos **19**, 033143 (2009).

[16] K. Murali and M. Lakshmanan, Phys. Rev. E **49**, 4882 (1994).

[17] N. F. Rulkov, M. M. Sushchik, L. S. Tsimring, and H. D. I. Abarbanel, Phys. Rev. E **51**, 980 (1995).

[18] H. Fujisaka and T. Yamada, Prog. Theor. Phys. **69**, 32 (1983).

[19] M. G. Rosenblum, A. S. Pikovsky, and J. Kurths, Phys. Rev. Lett. **76**, 1804 (1996); *ibid.* **78**, 4193 (1997).

[20] A. Pikovsky, M. Rosenblum, and J. Kurths, *Synchronization: A Universal Concept in Nonlinear Sciences* (Cambridge University Press, Cambridge, 2001).

[21] P. Bergé, Y. Pomeau, and C. Vidal, *L'ordre dans le chaos* (Hermann, Paris, 1988).

[22] M. Dubois, M. A. Rubio, and P. Bergé, Phys. Rev. Lett. **51**, 1446 (1983).

[23] N. Platt, E. A. Spiegel, and C. Tresser, Phys. Rev. Lett. **70**, 279 (1993).

[24] J. F. Heagy, N. Platt, and S. M. Hammel, Phys. Rev. E **49**, 1140 (1994).

[25] S. Boccaletti and D. L. Valladares, Phys. Rev. E **62**, 7497 (2000).

[26] M. Zhan, G. W. Wei, and C. H. Lai, Phys. Rev. E **65**, 036202 (2002).

[27] A. E. Hramov and A. A. Koronovskii, Europhys. Lett. **70**, 169 (2005).

[28] A. Pikovsky, M. Zaks, M. Rosenblum, G. Osipov, and J. Kurths, Chaos **7**, 680 (1997).

[29] K. J. Lee, Y. Kwak, and T. K. Lim, Phys. Rev. Lett. **81**, 321 (1998).

[30] S. Boccaletti, E. Allaria, R. Meucci, and F. T. Arecchi, Phys. Rev. Lett. **89**, 194101 (2002).

[31] E. J. Rosa, E. Ott, and M. H. Hess, Phys. Rev. Lett. **80**, 1642 (1998).

[32] Y. Pomeau and P. Manneville, Commun. Math. Phys. **74**, 189 (1980).

[33] C. Grebogi, E. Ott, F. Romeiras, and J. A. Yorke, Phys. Rev. A **36**, 5365 (1987).

[34] S. X. Qu, S. Wu, and D. R. He, Phys. Rev. E **57**, 402 (1998).

[35] P. Ashwin, E. Covas, and R. Tavakol, Nonlinearity **9**, 703 (1996).

[36] A. Prasad and R. Ramaswamy, Phys. Rev. E **60**, 2761 (1999).

[37] S. Dutta and R. Ramaswamy, J. Statist. Phys. **113**, 283 (2003).

[38] Y. Kuramoto and D. Battogtokh, Coexistence of Coherence and Incoherence in Nonlocally Coupled Phase Oscillators, Nonlinear Phenom. Complex Syst. **5**, 380 (2002).

[39] D. M. Abrams and S. H. Strogatz, Phys. Rev. Lett. **93**, 174102 (2004).

[40] M. J. Panaggio and D. M. Abrams, Nonlinearity **28**, R67 (2015).

[41] P. Ashwin and O. Burylko, Chaos **25**, 013106 (2015).

[42] M. J. Panaggio, D. M. Abrams, P. Ashwin, and C. R. Laing, Phys. Rev. E **93**, 012218 (2016).

[43] C. Bick and P. Aswin, Nonlinearity **29**, 1468 (2016).

[44] C. Bick, J. Nonlinear Sci. **27**, 605 (2017).

[45] F. Böhm, A. Zakharova, E. Schöll, and K. Lüdge, Phys. Rev. E **91**, 040901(R) (2015); A. Röhm, F. Böhm, and K. Lüdge, *ibid.* **94**, 042204 (2016).

[46] J. D. Hart, K. Bansal, T. E. Murphy, and R. Roy, Chaos **26**, 094801 (2016).

[47] D. Dudkowski, J. Grabski, J. Wojewoda, P. Perlikowski, Y. Maistrenko, and T. Kapitaniak, Sci. Rep. **6**, 29833 (2016).

[48] J. Wojewoda, K. Czolczynski, Y. Maistrenko, and T. Kapitaniak, Sci. Rep. **6**, 34329 (2016).

[49] Y. Maistrenko, S. Brezetsky, P. Jaros, R. Levchenko, and T. Kapitaniak, Phys. Rev. E **95**, 010203 (2017).

[50] V. K. Chandrasekar, R. Gopal, A. Venkatesan, and M. Lakshmanan, Phys. Rev. E **90**, 062913 (2014).

[51] R. Gopal, V. K. Chandrasekar, A. Venkatesan, and M. Lakshmanan, Phys. Rev. E **89**, 052914 (2014).

[52] N. Punetha, S. R. Ujjwal, F. M. Atay, and R. Ramaswamy, Phys. Rev. E **91**, 022922 (2015).

[53] S. R. Ujjwal, N. Punetha, and R. Ramaswamy, Phys. Rev. E **93**, 012207 (2016).

[54] H. Sakaguchi, Phys. Rev. E **73**, 031907 (2006).

[55] C. R. Laing, Phys. Rev. E **81**, 066221 (2010).

[56] G. C. Sethia, A. Sen, and F. M. Atay, Phys. Rev. Lett. **100**, 144102 (2008).

[57] G. C. Sethia and A. Sen, Phys. Rev. Lett. **112**, 144101 (2014).

[58] S. R. Ujjwal, N. Punetha, R. Ramaswamy, M. Agarwal, and A. Prasad, Chaos **26**, 063111 (2016).

[59] A. A. Khatun and H. H. Jafri, Commun. Nonlinear Sci. Numer. Simulat. **95**, 105661 (2021).

[60] A. A. Khatun, H. H. Jafri, and N. Punetha, Phys. Rev. E **103**, 042202 (2021).

[61] T. T. Wontchui, J. Y. Effa, H. P. E. Fouda, S. R. Ujjwal, and R. Ramaswamy, Phys. Rev. E **96**, 062203 (2017).

[62] J. B. Gao and Z. M. Zheng, Phys. Lett. A **181**, 153 (1993).

[63] J. B. Gao and Z. M. Zheng, Phys. Rev. E **49**, 3807 (1994).

[64] S. H. Strogatz, *Nonlinear Dynamics and Chaos: With Applications to Physics, Biology, Chemistry, and Engineering* (Perseus Books, New York, 1994).

[65] F. Takens, *Detecting Strange Attractors in Turbulence, Lecture Notes in Mathematics* (Springer, New York, 1981), Vol. 898.

[66] T. Sauer, J. Yorke, and M. Casdagli, J. Stat. Phys. **65**, 579 (1991).

[67] G. L. Baker, J. A. Blackburn, and H. J. T. Smith, Phys. Rev. Lett. **81**, 554 (1998).

[68] S. S. Sastry, *Introductory Methods of Numerical Analysis* (PHI Learning, New Delhi, India, 2012); A. Clauset, C. R. Shalizi, and M. E. Newman, SIAM Rev. **51**, 661 (2009).

[69] D. Dudkowski, Y. Maistrenko, and T. Kapitaniak, Chaos **26**, 116306 (2016).

[70] Y. L. Maistrenko, A. Vasylenko, O. Sudakov, R. Levchenko, and V. L. Maistrenko, Int. J. Bifurcation Chaos **24**, 1440014 (2014).

[71] D. J. Watts and S. H. Strogatz, Nature (London) **393**, 440 (1998).

[72] A. Erdős and P. Rényi, On the evolution of random graph, Publ. Math. Inst. Hung. Acad. Sci. **5**, 38 (1960).

[73] A.-L. Barabási and R. Albert, Science **286**, 509 (1999).

[74] M. G. Clerc, M. A. Ferré, S. Coulibaly, R. G. Rojas, and M. Tlidi, Opt. Lett. **42**, 2906 (2017).

[75] L. Schmidt, K. Schonleber, K. Krischer, and V. Garcia-Morales, Chaos **24**, 013102 (2014).

[76] S. Olmi, E. A. Martens, S. Thutupalli, and A. Torcini, Phys. Rev. E **92**, 030901(R) (2015).

[77] J. Singha and N. Gupte, Phys. Lett. A **384**, 126225 (2020).